Pakistan Veterinary Journal

ISSN: 0253-8318 (PRINT), 2074-7764 (ONLINE)
HTTPS://DOI.ORG/10.29261/pakvetj/2026.046

RESEARCH ARTICLE

Evaluation of Hepatic Injury and Regeneration After Lipiodol-Only Embolization in Normal Rabbit Liver Using 3T Dynamic-Enhanced MRI and Histopathology

So-Hyeon Park[1], Eunryel Nam[2], Bumseok Kim[3], Kichang Lee[1] and Hakyoung Yoon[1,4*]

[1]Department of Veterinary Medical Imaging, College of Veterinary Medicine, Jeonbuk National University, Iksan-si, Republic of Korea; [2]Laboratory of Companion Animal Surgery, Division of Small animal Clinic Sciences, Department of Veterinary Medicine, Rakuno Gakuen University, Japan; [3]BiosafetyResearch Institute and College of Veterinary Medicine, Jeonbuk National University, Iksan, Republic of Korea; [4]Institute of Animal Transplantation, Jeonbuk National University, Iksan 54596, Jeollabuk-do, Korea
*Corresponding author: knighttt7240@gmail.com

ARTICLE HISTORY (25-1110)

Received: November 15, 2025
Revised: January 25, 2026
Accepted: January 29, 2026
Published online: February 02, 2026

Key words:
Embolic material
Functional MRI
Hepatic perfusion imaging
Intra-arterial embolization
Ischemic injury

A B S T R A C T

Trans-arterial embolization (TAE) selectively embolizes the hepatic artery to block liver perfusion and is widely used for the treatment of hepatic tumors, traumatic hemorrhage, and vascular malformations. The aim of this study was to evaluate the early hepatic effects of lipiodol-only embolization at partial stasis, independent of additional embolic or chemotherapeutic agents in a rabbit model using imaging and histological examination. Nineteen New Zealand female rabbits were used; six were assigned to a pilot study for imaging protocol validation. Of the remaining 13 rabbits, three received normal saline (control), while 10 underwent lipiodol treatment (Group L) via the proper hepatic artery to evaluate hepatic changes. Computed tomography (CT), conventional magnetic resonance imaging (MRI), gadoxetate-enhanced MRI, and dynamic contrast-enhanced MRI (DCE-MRI) were performed before, immediately after, and 24-h post-embolization. In the Group L, unlike conventional MRI, gadoxetate-enhanced MRI demonstrated a significant decrease ($P<0.05$) in signal intensity immediately and 24-h post-embolization. On DCE-MRI, K_{trans}, $iAUC_{60}$, CER, Max. slope, PEI and TTP showed significant differences between pre- and immediately post-embolization and between immediate and 24-h post-embolization ($P<0.05$, Wilcoxon signed-rank test), but not between pre- and 24-h post-embolization. Histologically, the median total Suzuki score was higher ($P<0.05$) in Group L [5 (4–6)] than in controls [0 (0–1)]. The Ki-67 proliferation index was also higher in Group L [23.61 (17.14–27.54)] than in controls [2.14 (1.78–3.26)] ($P<0.05$). Based on DCE-MRI and histopathologic findings, clinically relevant lipiodol dose (0.1mL/kg) induced transient hepatic injury and perfusion changes in normal liver, with partial recovery by 24h. DCE-MRI was most sensitive in detecting these dynamic changes, suggesting that DCE-MRI may serve as a non-invasive imaging marker for assessing hepatic injury and recovery following embolization.

To Cite This Article: Park SH, Nam E, Kim B, Lee K and Yoon H, 2026. Evaluation of hepatic injury and regeneration after lipiodol-only embolization in normal rabbit liver using 3t dynamic-enhanced mri and histopathology. Pak Vet J, 46(3): 575-586. http://dx.doi.org/10.29261/pakvetj/2026.046

INTRODUCTION

Trans-arterial embolization (TAE) is an interventional procedure that selectively embolizes the hepatic artery to block liver perfusion and is widely used for the treatment of hepatic tumors, traumatic hemorrhage, and vascular malformations in both human and veterinary medicine (Mahmoodiyan and Mahboubizadeh, 2025). However, because a normal liver receives part of its blood supply from the arteries, nontarget ischemic damage can occur if the embolic material reaches the adjacent normal liver parenchyma (Zaarou *et al.*, 2024). This damage can remarkably affect liver function and clinical outcomes, especially in patients with impaired liver function.

Lipiodol, an oil-based contrast agent, is commonly used in combination with embolic particles, but its use alone is preferred in cases of portal vein invasion (Lawson *et al.*, 2023). Post-procedure monitoring using imaging modalities such as contrast-enhanced computed tomography (CT) or magnetic resonance imaging (MRI)

plays an important role in assessing the effectiveness of treatment, degree of damage to the surrounding liver tissue, and determining the need for additional treatment. Imaging follow-up is essential not only to detect tumor progression or recurrence, but also to ensure optimal timing and strategy for second-line embolization (Sharma *et al.*, 2020).

Computed tomography has long been considered as the standard imaging technique for post-TAE monitoring because it can visualize lipiodol and overall treatment response. However, the high attenuation of lipiodol on CT obscures residual viable tumor tissue or complicate the assessment of necrosis and tumor recurrence. Recent studies have shown that MRI, with its high soft tissue contrast and lack of lipiodol interference, can better detect residual viable tissue (Ozaki *et al.*, 2026). Also, some reports suggest that the lipiodol area does not correspond to the actual necrotic area, suggesting that lipiodol distribution does not always accurately reflect the extent of necrosis (Kubota *et al.*, 2001).

Gadoxetic acid-enhanced MRI utilizes gadoxetate disodium, a hepatocyte-specific contrast agent that rapidly enters the extracellular spaces and functional hepatocytes (Lee *et al.*, 2022). Approximately 50% of the injected gadoxetate disodium is excreted via the biliary tract, and the remaining 50% via the kidneys. Consequently, gadoxetic acid-enhanced MRI provides both anatomical and functional information, helping to evaluate liver function, tumor vascularity, vascular and biliary anatomy, and bile leakage (Baleato-González *et al.*, 2023). Decreased transport of gadoxetate disodium during the hepatobiliary phase appears in the form of hypointensity, which indicates hepatocyte dysfunction and helps in predicting the outcome of treatment.

However, gadoxetic acid-enhanced MRI has limitations in detecting rapid or subtle perfusion changes immediately after embolization. Therefore, dynamic enhanced MRI (DCE-MRI) has emerged as a promising technique for assessing early hemodynamic changes in liver tissue and residual tumor (Rata *et al.*, 2021). DCE-MRI quantitatively measures parameters such as hepatic blood flow, blood volume, and mean transit time. So, it is useful for assessing acute perfusion changes, compensatory redistribution, and early liver regeneration, which are difficult to observe with conventional or gadoxetate-enhanced MRI.

While a reasonable number of studies have focused on tumor response and dose-dependent toxicity (Wang *et al*., 2011; Deschamps *et al*., 2017) to TAE, studies examining the effects of lipiodol on normal liver tissue remain limited (Keller *et al.*, 2020). As liver failure after TAE is often due to damage to the functional liver parenchyma rather than tumor progression (Huang *et al.*, 2002, Baleato-González et al., 2023), a better understanding of effects of lipiodol on normal liver tissue is essential. Lipiodol may inadvertently reach non-target liver areas because of reflux, proximal arterial embolization, or incorrect catheter placement (Kacala *et al.*, 2023). Even when ultra-selective embolization is achieved, ischemic injury can extend to the peritumoral non-tumorous parenchyma (Miyayama *et al.*, 2009). Despite these clinically relevant risks, few studies have comprehensively assessed early imaging changes in normal hepatic tissue after embolization.

This study aimed to investigate the early hepatic effects of lipiodol-only embolization at partial stasis, independent of additional embolic or chemotherapeutic agents. It was hypothesized that lipiodol-only embolization would induce transient but detectable hepatic injury in non-tumorous liver tissue, which could be characterized using multimodal imaging and histological analysis.

MATERIALS AND METHODS

Animal and grouping: A total of 19 clinically healthy, female New Zealand rabbits (90–105 days old, 2.78±0.31kg BW) were provided for this study by the Laboratory Animal Research Center, Jeollabuk-do, Republic of Korea. These experimental rabbits were individually housed under standardized, temperature-controlled conditions with free access to food and water. This study was conducted between October 2024 and April 2025 and was approved by the Institutional Animal Care and Use Committee of Jeonbuk National University (JBNU NON2024-157). Six rabbits were used in a pilot study; three as controls, while 10 underwent lipiodol embolization (Group L). The small sample size in control group (n=3) was chosen to minimize unnecessary animal use in line with ethical principles, and is already supported by previous studies showing that intra-arterial saline infusion alone does not induce significant hepatic or systemic changes in rabbits (Zhang *et al.,* 2022).

Pilot study: A pilot study was carried out to evaluate whether residual gadoxetate disodium (0.025mmol/kg; Primovist, Bayer, Germany) affected DCE-MRI parameters in six rabbits. Rabbits underwent the same anesthesia protocol as the main study but did not receive embolization. Rabbits first underwent DCE-MRI with gadolinium (0.1mmol/kg of Gadovist, Guerbet, France), and after 3-day washout received gadoxetate disodium, followed by gadolinium 15 minutes later (hepatobiliary phase), as described earlier (Breit *et al*, 2023). DCE-MRI parameters including volume transfer constant (K_{trans}), extravascular extracellular volume fraction (V_e), increased area under the curve ($iAUC_{60}$), maximum slope (Max. slope), contrast enhancement ratio (CER), Positive enhancement integral (PEI), Time to peak (TTP) and Mean time to enhance (MTE) were recorded and compared for imaging protocol validation.

Anesthesia and embolization: Anesthesia in experimental rabbits was induced with acepromazine (0.5mg/kg) and meloxicam (0.1mg/kg) subcutaneously, followed by isoflurane inhalation. Cefazoline (20mg/kg) was injected, and anesthesia was maintained with isoflurane (1–2%) through a V-gel. For vascular access in rabbits of control and Group L, A 4 Fr vascular sheath was inserted into the femoral artery. The celiac artery was catheterized with a 4 Fr angio-catheter and 0.035" guidewire. Arteriography was performed with iohexol (300mg I/mL; 2 mL/kg). The proper hepatic artery (PHA) was catheterized with a 1.5 Fr microcatheter and 0.014" microguidewire (Ning and Wang, 2020). Rabbits of control group received 0.3ml saline per rabbit, while those of Group L received lipiodol (0.1ml/kg) via the PHA (Nakao *et al.*, 1994).

Imaging protocol: Computed Tomography and MRI were performed at pre-, immediate post-embolization, and 24h

post-embolization. For CT, a 16-slice scanner (Alexion Advance; Toshiba Medical Systems, Japan) was used. Arterial phase was acquired via bolus tracking in the right ventricle, followed by portal venous and delayed phases at 30s and 55s. Region of interest (ROI; $1cm^2$) was placed in each lobe, avoiding major vessels; mean Hounsfield unit (HU) ratio was calculated as follows (Nagayama *et al*., 2021):

$$\text{HU ratio (\%)} = \left(\frac{HU_{phase} - HU_{pre}}{HU_{pre}}\right) \text{x } 100$$

For MRI, a 3-T scanner (uMR 780, United Imaging Healthcare, China) with a 12-channel super-flexed and an 8-channel spine coils was used. Sequences included T1-weighted fat-saturated (T1-W_fs), Dixon-based dual-echo T1-weighted (T1-W_dual), T2-weighted image with (T2-W_fs) and without fat-saturated (T2-W), and Acquisition and reconstruction with motion suppression diffusion-weighted imaging (ARMS_DWI) with b value of 100 or 300s/mm^2 (Table 1). Proton density fat fraction (PDFF, %) was estimated using a dual-echo Dixon method based on the SI of the in-phase (S_{IP}) and opposed-phase (S_{OP}), as follows (Reeder *et al.,* 2011):

$$\text{PDFF (\%)} = \frac{|S_{IP} - S_{OP}|}{2S_{IP}} \times 100$$

In the Gadoxetate-enhanced MRI using gadoxetate disodium (0.025mmol/kg), arterial phase conducted 5s post-injection, followed by five sequential dynamic phases and a 15min hepatobiliary phase. Signal intensity (SI) change was calculated as described earlier (Chen *et al*., 2014):

$$\text{SI change (\%)} = \left(\frac{|SI_{phase} - SI_{baseline}|}{SI_{baseline}}\right) \times 100$$

Table 1: Parameters of MRI sequences

	T1-W_fs*	T1-W dual-echo	T2-W_fs	T2-W	ARMS_DWI	DCE-MRI
TR (ms)	4	7	2525	2344	3527	3
TE (ms)	2	2	74	74	96	1
Field of view (cm)	180×180	180×180	180×180	180×180	180×180	150×115
Matrix	144×144	160×128	192×192	192×192	96×96	48×37
Slice space (mm)	1.0	1.0	3.6	3.6	4.08	1.75
Slice thickness (mm)	1.0	1.0	3.0	3.0	3.4	1.75
Flip angle (^{0})	13	10	135	135	73	10

T1-W_fs; T1-weighted fat-saturated sequence, T1-W_dual; Dixon-based dual-echo T1-weighted sequence, T2-W_fs; T2-weighted fat-saturated sequence, T2-W_fs; T2-weighted sequence. TR; Repetition time, TE; Echo time. *T1-W_fs was also used in gadoxetate-enhanced MRI

In the DCE-MRI using gadolinium (0.1mmol/kg), volume transfer constant (K_{trans}) and extravascular extracellular volume fraction (V_e) were calculated by extended Tofts model (Reynolds *et al*., 2022). Semi-quantitative parameters included increased area under the curve ($iAUC_{60}$), maximum slope (Max. slope), contrast enhancement ratio (CER), Positive enhancement integral (PEI), Time to peak (TTP) and Mean time to enhance (MTE).

Blood and histopathological analysis: At 24h post-embolization, 1mL of blood was collected from the auricular vein of rabbits in control and lipiodol groups, and divided into two parts; one with EDTA for hematological parameters (RBC, WBC, HCT) and one without anticoagulant for serum biochemistry parameters including aspartate aminotransferase (AST), alanine aminotransferase (ALT), alkaline phosphatase (ALP) and gamma-glutamyl transferase (GGT). Serum was centrifuged and analyzed (NX700, Fujifilm, Japan) with Fujifilm assay kits for AST (Cat. No. 3150), ALT (Cat. No. 3250), ALP (Cat. No. 3550), and GGT (Cat. No. 3050). At 24h post-embolization, rabbits in the control group and Group L were euthanized under deep anesthesia with isoflurane, and liver tissues were excised. Samples were fixed in formalin, paraffin-embedded and stained with H&E and Ki-67 (MIB-1; Dako, USA). Liver injury was graded on H&E stain via Suzuki score (0–4 for congestion, vacuolar degeneration and necrosis) across six 100× fields (Liang *et al*., 2022). The Ki-67 proliferation index was calculated on immunostained sections as the percentage of positive hepatocytes in six 200× fields (de Graaf *et al*., 2011).

Statistical analysis: Data were expressed as median with IQRs (Shapiro-Wilk test), excluding histopathological parameters. Wilcoxon signed-rank test assessed within-group differences across timepoints. Because the data on total Suzuki score and Ki-67 proliferation index were not normally distributed, showed floor effects in the control group, and involved a small sample size, comparisons between the control group and Group L were performed using the non-parametric Mann–Whitney U test. P<0.05 was considered significant. Statistical package SPSS v20 (IBM) was used for statistical analysis.

RESULTS

Pilot study: Results of the pilot study revealed that the sequential administration significantly reduced $iAUC_{60}$, maximum slope, CER, and PEI compared with gadolinium alone (P<0.05). In contrast, K_{trans}, V_e, TTP, and MTE showed statistically non-significant differences between Sequential administration and Gadolinium alone (Table 2).

Table 2: Comparison of signal intensity changes between sequential gadoxetate-gadolinium administration and gadolinium alone (Pilot study)

Parameter (unit)	Sequential administration Median (IQR)	Gadolinium alone Median (IQR)	P value
K_{trans} (min^{-1})	0.95 (0.83-1.00)	0.99 (0.88-1.29)	>0.05^{NS}
V_e	0.10 (0.09-0.11)	0.12 (0.07-0.15)	>0.05^{NS}
$iAUC_{60}$ (min · mmol/l/100)	2.99 (2.96-3.61)	9.66 (8.84-12.53)	<0.05*
Max. slope (mmol/min)	0.37 (0.34-0.41)	1.63 (1.30-1.91)	<0.05*
CER	0.34 (0.32-0.36)	1.14 (0.82-1.58)	<0.05*
TTP (s)	35.43 (25.98-38.38)	30.25 (25.02-38.67)	>0.05^{NS}
PEI	736.92 (650.78-846.36)	1251.01 (1141.67-1400.29)	<0.05*
MTE (s)	27.87 (27.17-29.27)	27.75 (26.35-31.12)	>0.05^{NS}

K_{trans}, volume transfer contrast; V_e, extravascular extracellular volume fraction; AUC, area under the curve; Max. slope, maximal slope; CER, contrast enhancement ratio; TTP, time to peak; PEI, positive enhancement integral; MTE, mean time to enhance. *Significant (P<0.05); ^{NS}Non-significant.

Embolization: In group L, partial stasis was observed, characterized by residual arterial perfusion following embolic material administration (Fig. 1A–D). Fig. 1A shows angiography obtained after contrast injection through an angiocatheter placed in the celiac artery, demonstrating distinct intrahepatic arterial flow. Fig. 1B illustrates advancement of the microcatheter into the proper hepatic artery. Fig. 1C depicts lipiodol injection through the microcatheter, while Fig. 1D presents the post-embolization angiogram showing reduced intrahepatic arterial flow compared with the pre-embolization image. The total procedure time was approximately 60 min.

Imaging findings

Comparative CT findings: In group L, Hyper-attenuated lipiodol deposition was clearly observed within the hepatic parenchyma, confirming successful embolization at the pre-contrast image (Fig. 2A). During the arterial phase (Fig. 2B), hepatic parenchymal enhancement was minimal, as the normal liver receives the majority of its blood supply from the portal vein. In the portal venous phase (Fig. 2C), the hepatic parenchyma appeared slightly more hyper-attenuated than in the arterial phase, but the degree of enhancement was lower than that seen before embolization. There was complete opacification of the portal vein and partial filling of the caudal vena cava. In the delayed phase (Fig. 2D), liver exhibited diffusely decreased enhancement, consistent with perfusion reduction following embolization. There was full contrast in caudal vena cava and intrahepatic vein.

In group L (Fig. 3A), HU values significantly decreased across all contrast-enhancement phases immediately after embolization, except the arterial phase ($P<0.05$). The Wilcoxon signed-rank test revealed significant HU changes between immediate post- and 24-h post-embolization only in the pre-contrast and arterial phases ($P<0.05$). When comparing pre- and 24-h post-embolization, significant differences were observed in all phases except the arterial phase ($P<0.05$). In the control group with n=3, (Fig. 3B), Wilcoxon signed-rank test revealed statistically non-significant differences in CT parameters across the three-time points (pre-, immediate post-, and 24h post-embolization).

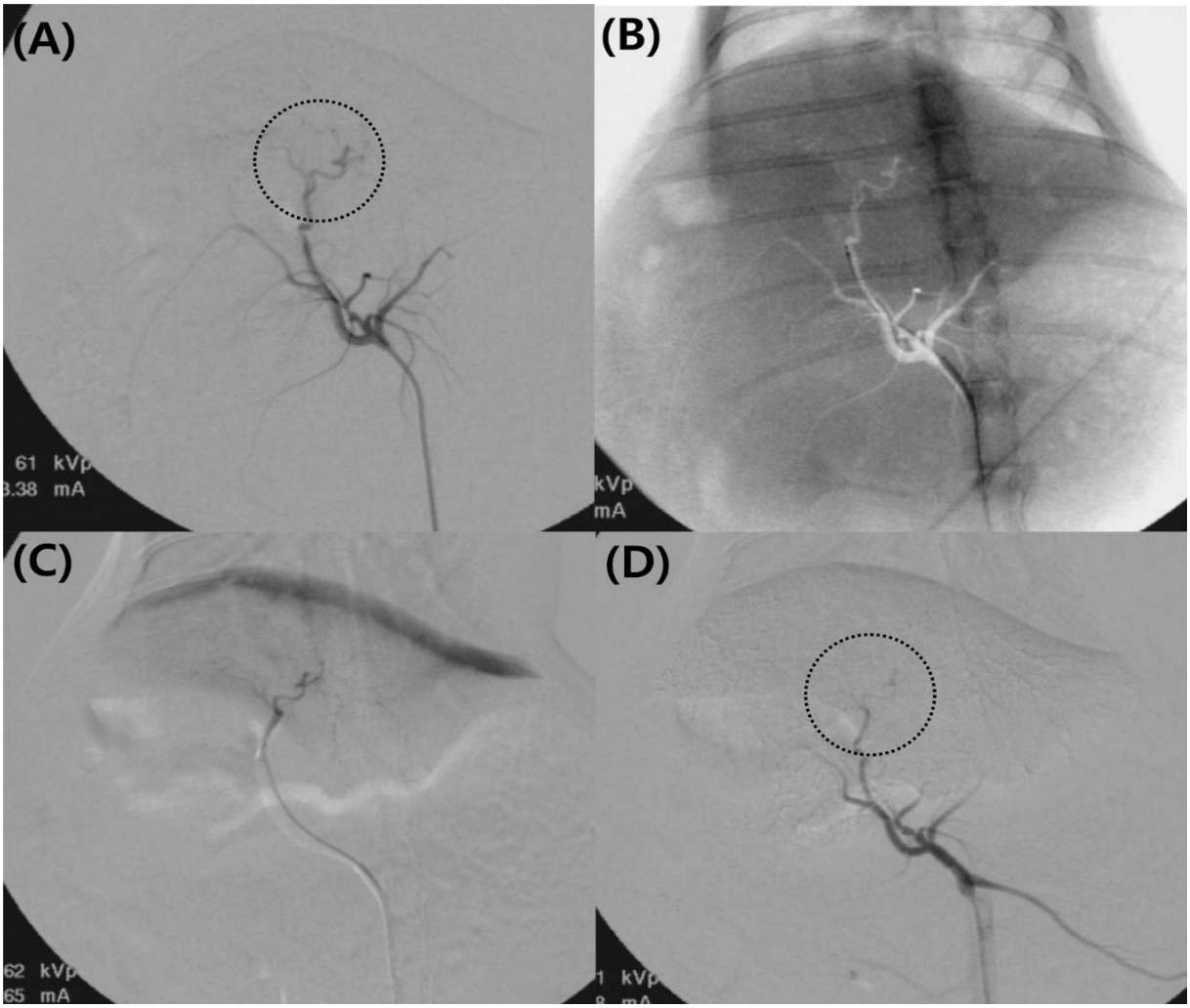

Fig. 1: Representative fluoroscopic images showing partial arterial stasis in Group L, characterized by delayed but continuous residual arterial perfusion following embolization. (A): Angiography obtained after contrast injection via an angiocatheter positioned in the celiac artery, showing distinct intrahepatic arterial flow (dotted circle). (B): Microcatheter advanced through the angiocatheter and positioned in the PHA. (C): Image captured during lipiodol injection via the microcatheter. (D): Post-embolization angiography following microcatheter removal, demonstrating reduced intrahepatic arterial flow compared to the pre-embolization image (dotted circle).

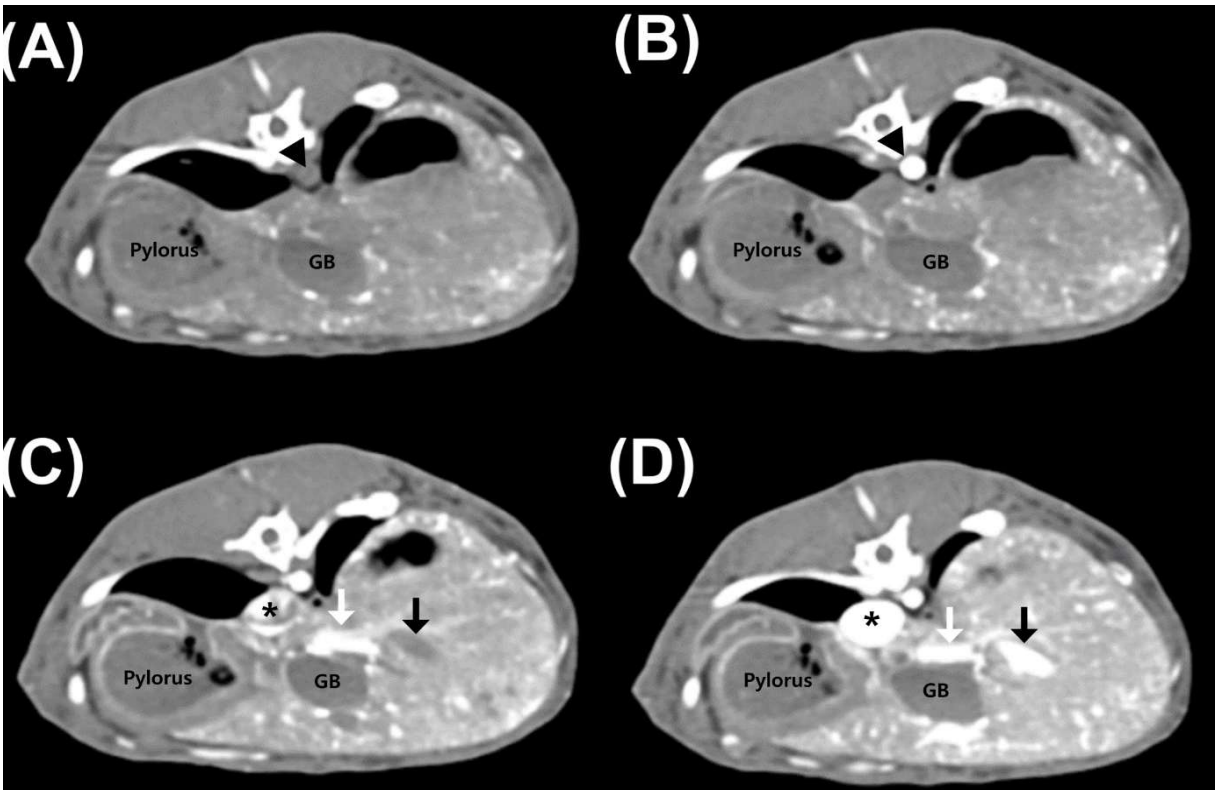

Fig. 2: CT images showing: (A): Pre-contrast phase showing hyperattenuated lipiodol deposition (arrow-head) in the hepatic parenchyma, GB; gall bladder. (B): Arterial phase with aortic contrast opacification (arrow-head); hepatic parenchymal enhancement is minimal, reflecting predominant portal perfusion in normal liver tissue. (C): Portal venous phase showing complete opacification of the portal vein (white arrow) and partial filling of the caudal vena cava (star); hepatic parenchyma enhancement is lower than pre-embolization. (D): Delayed phase with full contrast in caudal vena cava (star) and intrahepatic vein (black arrow); overall hepatic enhancement is decreased, reflecting perfusion reduction post-embolization. Portal vein is shown by the white arrow.

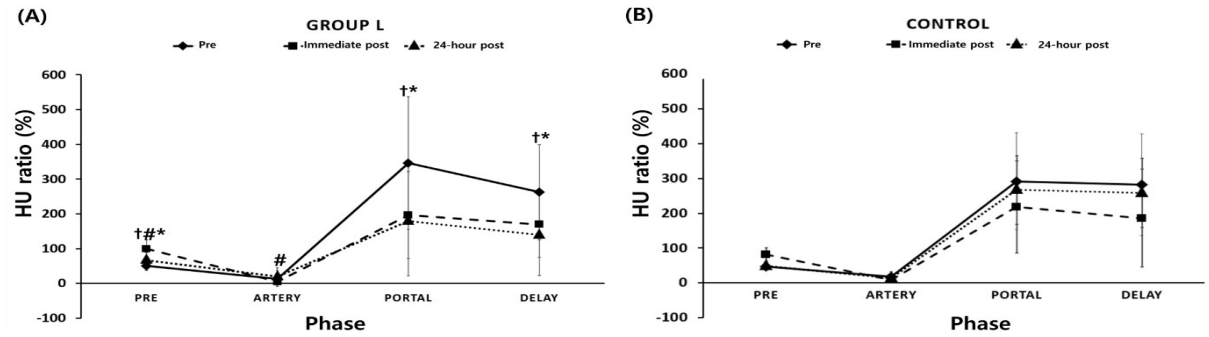

Fig. 3: Hounsfield unit (HU) ratio across CT phases pre-, immediate post-, and 24-ho post-embolization in Group L (A) and control group (B). Group L data are shown as median (IQR), and control data as median (min-max). Pre-embolization, solid line with rhombus; immediate post-embolization, dashed line with the rectangle; 24-h post-embolization, dotted line with the triangle. †P<0.05, pre- vs. immediate post-embolization; #P<0.05, immediate post- vs. 24-h post-embolization; *P<0.05, pre- vs. 24-h post-embolization.

Comparative MRI findings:

Conventional MRI (T1-, T2-, and dual-phase sequences) and DWI findings: On visual assessment, immediately after embolization, no significant signal changes were observed in any case across all MRI sequences. At 24-h post-embolization, hypointense signal changes were observed in two cases: one case on T2-W_fs (Fig. 4D) compared with pre-embolization (Fig. 4C), and another case on T1-W_fs (Fig. 4J) compared with pre-embolization (Fig. 4I). In the remaining cases at 24-h post-embolization, lesions appeared isointense on T2-W_fs (Fig. 4L) compared with pre-embolization (Fig. 4K) and on T1-W_fs (Fig. 4B) compared with pre-embolization (Fig. 4A). In all cases, post-embolization DWI (Figs. 4G & 4O) and ADC (Figs. 4H & 4P) remained isointense compared with pre-embolization DWI (Figs. 4E & 4M) and ADC (Figs. 4F & 4N).

No qualitative changes were observed on T1-W dual-phase images before and after embolization. In the control group, PDFF (%) remained stable over time, with non-significant changes observed between pre-, immediately post-, and 24h post-embolization. In contrast, Group L showed significantly elevated PDFF (%) values both immediately after embolization and at 24h post-embolization, compared to baseline (P<0.05), as determined by the Wilcoxon signed-rank test (Table 3).

Gadoxetate-enhanced MRI: Eight-phase SI changes: The Wilcoxon signed-rank test was performed to compare SI across different phases: pre- and immediate post-embolization, immediate and 24-h post-embolization, and pre- and 24-h post-embolization. At hepatobiliary phase (HBP), SI significantly decreased between the pre- and immediate post-embolization phases, as well as between the pre- and 24-h post-embolization phases ($P<0.05$, Fig. 5A). However, non-significant differences were observed between the immediate and 24-h post-embolization phases and across all eight phases. No bile leaks were observed in the hepatobiliary phase, and the biliary tract appeared intact throughout the examination.

DCE MRI findings: DCE parameters, including K_{trans}, V_e, $iAUC_{60}$, Max. slope, CER, PEI, TTP, and MTE were obtained. The mean SI changes of 10 rabbits in group L at each phase: pre-, immediate post-, and 24-h post-embolization are shown in Fig. 5B. The mean SI markedly decreased immediately after embolization and then increased at 24 hours post-embolization, approaching values similar to those observed at baseline.

Compared with pre-embolization, immediate post-embolization showed statistically significant decreases in K_{trans}, $iAUC_{60}$, CER, Max. slope and PEI, along with a significant increase in TTP ($P<0.05$). Between immediate and 24-h post-embolization, K_{trans}, $iAUC_{60}$, CER, Max. slope and PEI increased, whereas TTP significantly decreased. In contrast, V_e and MTE showed non-significant changes across all time points (Table 4). Non-significant difference was observed between pre- and 24-h post-embolization for all DCE parameters. In the control group (n=3), Wilcoxon signed-rank test revealed statistically non-significant differences in MRI parameters across the three-time points (Table 4).

Table 3: Quantitative changes in Proton density fat fraction (PDFF, %) at pre-, immediate post- embolization (Post 0), and 24-hour post-embolization (Post 1)

Phase	Control (n=3) Median (Min-Max)			Group L (n=10) Median (Q1-Q3)		
	Pre	Post 0	Post 1	Pre	Post 0	Post 1
PDFF (%)	5.62 (3.19-6.25)	5.28 (3.87-6.72)	5.37 (3.17-7.35)	4.33 (3.21-5.29)	6.32† (5.20-7.18)	5.26* (4.55-6.52)

†P<0.05 (pre- vs. immediate post-embolization, Wilcoxon rank test). *P<0.05 (pre- vs. 24-h post-embolization, Wilcoxon rank test).

Figure 6 shows a color map of the DCE parameters. In the color maps, colors closer to red represent higher values, whereas colors closer to purple or black indicate lower values. In Fig. 6A, the hypointense area in the hepatobiliary phase (dotted-line region) was considered to represent embolization-induced hepatic injury. This region demonstrated lower values (purple to black) than the surrounding liver parenchyma (solid-line region) on the K_{trans} (Fig. 6B), V_e (Fig. 6C), $iAUC_{60}$ (Fig. 6D), Max. slope (Fig. 6E), CER (Fig. 6F), and PEI maps (Fig. 6G). In contrast, the injured region showed higher values (close to red) on the TTP map (Fig. 6H) than on the surrounding liver parenchyma. No noticeable differences were observed for MTE (Fig. 6I).

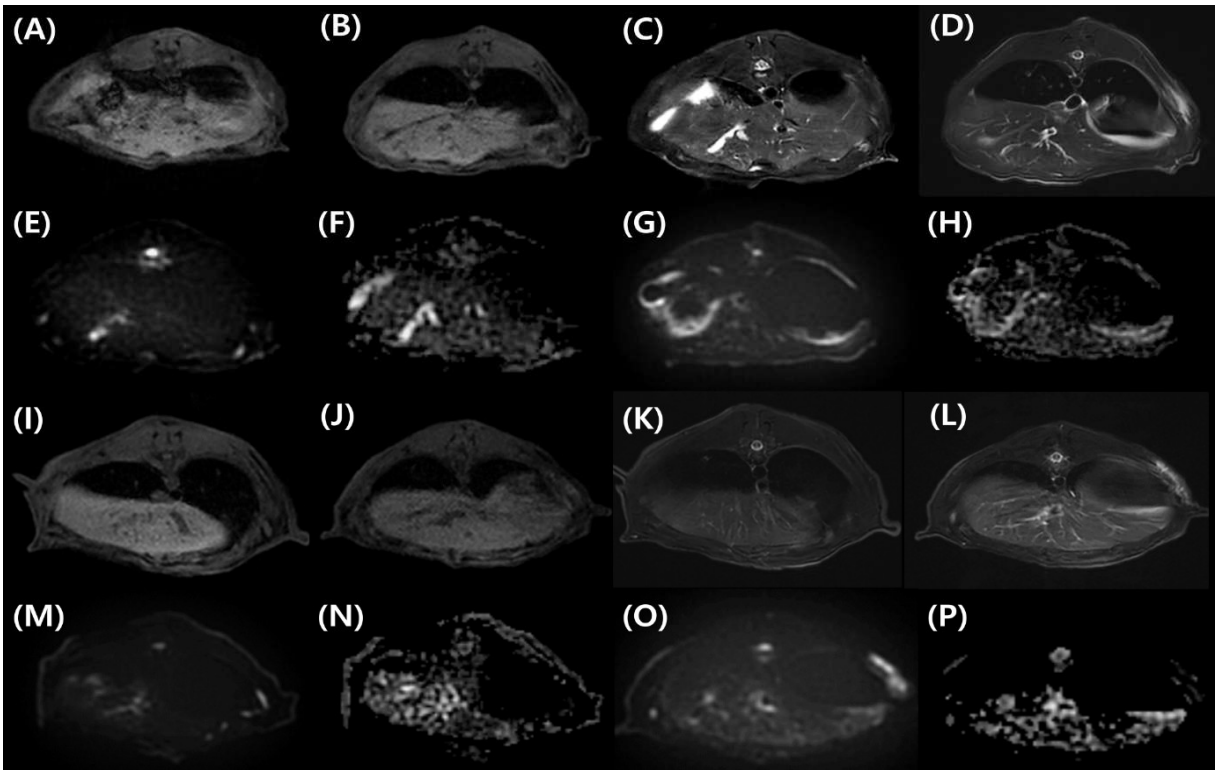

Fig. 4: Representative MRI images from two cases in Group L. In Case 1, pre-embolization images are shown in A, C, E and G; and 24-h post-embolization images in B, D, F and H. T1-weighted fat-suppressed (T1-W_fs) images (A & B) demonstrate isointense signals before and after embolization. T2-weighted fat-suppressed (T2-W_fs) images (C & D) show decreased signal intensity after embolization. Diffusion-weighted imaging (DWI; E & F) and apparent diffusion coefficient (ADC) maps (G & H) show no remarkable changes. In Case 2, pre-embolization images are shown in I, K, M and O; and 24-h post-embolization images are shown in J, L, N and P. T1-W_fs images (I & J) demonstrate hypointense changes after embolization, whereas T2-W_fs images (K & L), DWI (M & N), and ADC maps (O & P) show no apparent changes.

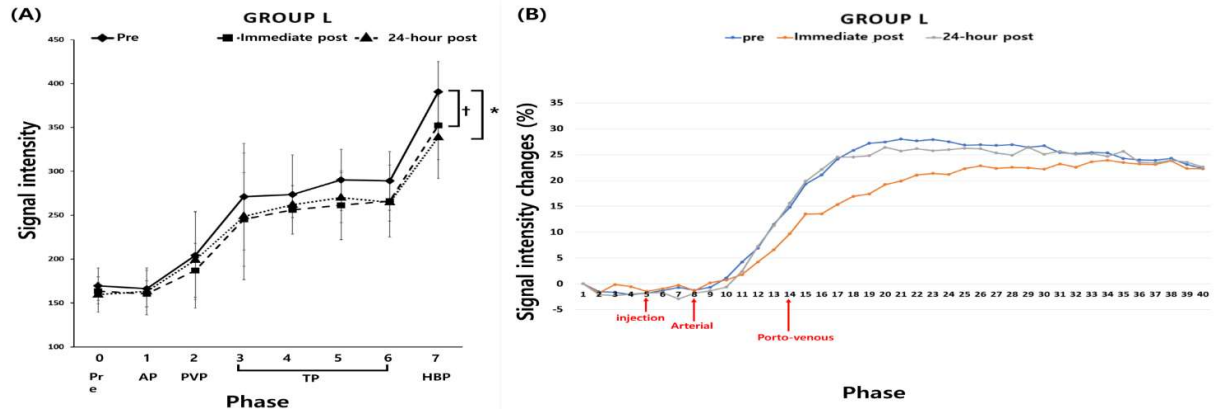

Fig. 5: Signal intensity changes on gadoxetate-enhanced MRI and signal intensity changes across phases in dynamic contrast-enhanced magnetic resonance images using gadolinium in Group L. (A): This graph illustrates the changes in signal intensity (arbitrary units) across discrete sequence of gadoxetate-enhanced MRI at three-time points: pre-, immediate post-, and 24-h post-embolization. This figure also illustrates phase-dependent enhancement with hepatocyte-specific contrast. Pre; pre-contrast, AP; arterial phase, PVP; portal venous phase, TP; transitional phase, HBP; hepatobiliary phase. †P<0.05 indicates significant difference between pre- and immediate post-embolization; *P<0.05 indicates significant difference between pre- and 24-h post-embolization. (B): Signal intensity changes are plotted on Y-axis (%) across continuous imaging phases on the X-axis (1-40), representing sequential temporal acquisition. This figure captures perfusion-related dynamic changes, reflected hepatic perfusion rather than discrete phase enhancement.

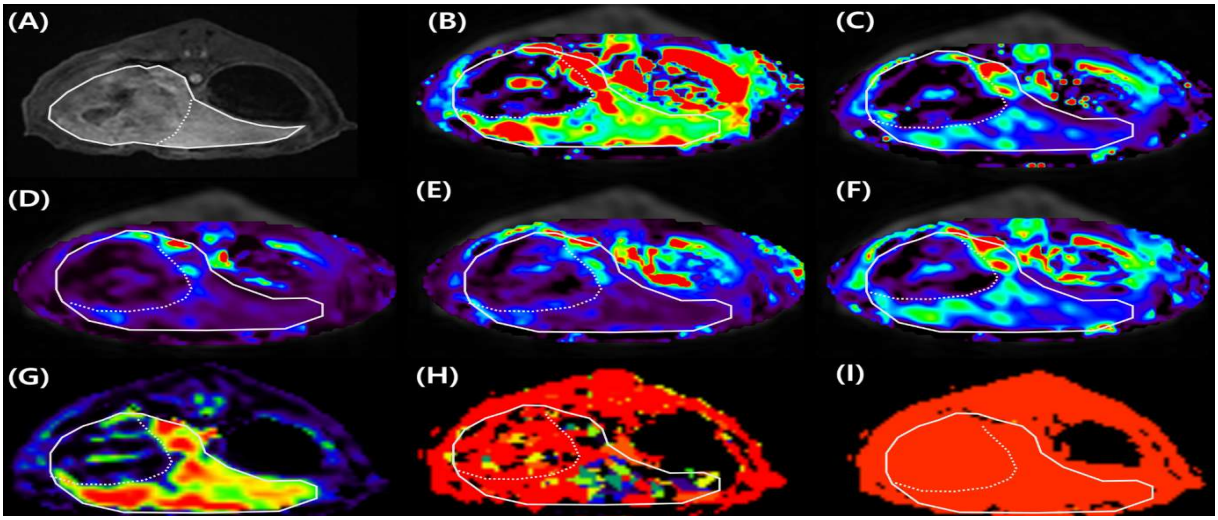

Fig. 6: Color maps of DCE parameters in Group L. (A): Hepatobiliary phase image obtained from gadoxetate-enhanced MRI. The solid-line region indicates hepatic parenchyma, while the dotted-line region shows areas of hypointensity, suggesting hepatic injury due to embolization. (B): $\boldsymbol{K_{trans}}$, (C): V_e, (D): $\boldsymbol{iAUC_{60}}$, (E): Max. slope, (F): Contrast enhancement ratio (CER), (G): Positive enhancement integral (PEI), (H): Time to peak (TTP), and (I): Mean time to enhance (MTE). In the color maps from DCE-MRI, red corresponds to higher values, and purple corresponds to lower values. Necrotic regions exhibited lower values (closer to purple) compared with normal parenchyma in $\boldsymbol{K_{trans}}$, V_e, $\boldsymbol{iAUC_{60}}$, Max. slope, CER and PEI. For TTP, the embolized region appeared closer to red, indicating higher values compared with normal hepatic tissue. No noticeable differences were observed for MTE.

Table 4: DCE-MRI parameters in the control group and Group L at pre-, immediate post-, and 24-h post-embolization

Parameter	Control (n=3) Median (Min-Max)			Group L (n=10) Median (Q1-Q3)		
	Pre	Post 0	Post 1	Pre	Post 0	Post 1
K_{trans} (min^{-1})	1.01 (0.88-1.12)	0.96 (0.90-1.02)	0.89 (0.84-1.13)	0.93 (0.89-1.20)	0.35† (0.29-0.47)	0.56# (0.43-1.61)
V_e	0.10 (0.09-0.13)	0.08 (0.04-0.15)	0.12 (0.06-0.14)	0.10 (0.06-0.26)	0.13 (0.09-0.18)	0.13 (0.10-0.26)
$iAUC_{60}$ (min · mmol/l/100)	3.02 (2.72-3.10)	2.97 (2.43-3.17)	2.86 (2.33-3.33)	3.09 (2.82-3.15)	2.25† (2.04-2.68)	2.94# (2.76-3.14)
Max. slope (mmol/min)	0.34 (0.27-0.36)	0.35 (0.29-0.43)	0.36 (0.24-0.41)	0.37 (0.28-0.50)	0.29† (0.26-0.33)	0.31# (0.28-0.39)
CER	0.33 (0.30-0.35)	0.35 (0.33-0.37)	0.34 (0.29-0.38)	0.35 (0.34-0.36)	0.32† (0.29-0.33)	0.33# (0.32-0.35)
TTP (s)	38.67 (35.64-41.06)	40.55 (39.25-40.92)	37.68 (36.67-39.67)	38.63 (36.11-38.96)	52.31† (48.06-55.95)	40.56# (31.27-46.76)
PEI	650.71 (591.9-718.17)	676.79 (595.82-872.56)	617.81 (607.92-680.59)	1099.35 (883.73-1180.50)	628.91† (492.74-774.53)	873.21# (658.11-1092.35)
MTE (s)	27.36 (24.6-29.49)	26.70 (21.26-31.26)	26.70 (21.26-31.26)	28.48 (25.92-29.02)	23.20 (19.48-27.60)	26.10 (20.55-31.13)

†P<0.05 (pre- vs. immediate post-embolization, Wilcoxon rank test). #P<0.05 (immediate vs. 24-h post-embolization, Wilcoxon rank test). Post 0, immediate post-embolization; Post 1: 24h post-embolization; K_{trans}, volume transfer contrast; V_e, extravascular extracellular volume fraction; AUC, area under the curve; Max. slope, maximal slope; CER, contrast enhancement ratio; TTP, time to peak; PEI, positive enhancement integral; MTE, mean time to enhance

Blood and histopathological analysis: In group L, following lipiodol administration, paired analysis using the Wilcoxon signed-rank test demonstrated significant increase in ALT and AST ($P<0.05$), compared to pre-treatment values, whereas ALP, GGT, WBC, RBC, and hematocrit (HCT) remained unchanged, indicating selective hepatic enzyme response (Table 5). In control group, although the sample size was small, the values remained stable over time, supporting the validity of saline for use as a negative control. Mild but non-significant elevation in liver enzyme levels (ALT, AST, and GGT) was observed 24h after intra-arterial infusion of normal saline into the hepatic artery, while ALP levels were consistently above the normal reference range. Despite this increasing trend, all enzyme levels were within the normal reference range except for ALP, with statistically non-significant differences (Table 5). Moreover, in control group, non-significant changes in RBC, WBC or HCT were observed after normal saline infusion.

In the control group, minimal liver injury was observed, and all three rabbits had Suzuki scores of 0, 0, and 1, indicating minimal liver damage. Gross (Fig. 7A) and cross-sectional liver images (Fig. 7B) revealed smooth liver surfaces without any gross lesions, and H&E staining (Fig. 7C) showed normal lobular structure without evidence of congestion, necrosis, or inflammatory infiltrates. Gross (Fig. 7E) and cross-sectional liver images (Fig. 7F) showed multiple small white-grey nodules. Conversely, Group L showed moderate hepatic congestion, cell edema, vacuolar degeneration, and mild-to-moderate hepatic necrosis on H&E staining (Fig. 7G). The median total Suzuki score in Group L was 5 (range, 4–6), which was significantly higher than that of the control group (0, range 0–1; $P<0.05$).

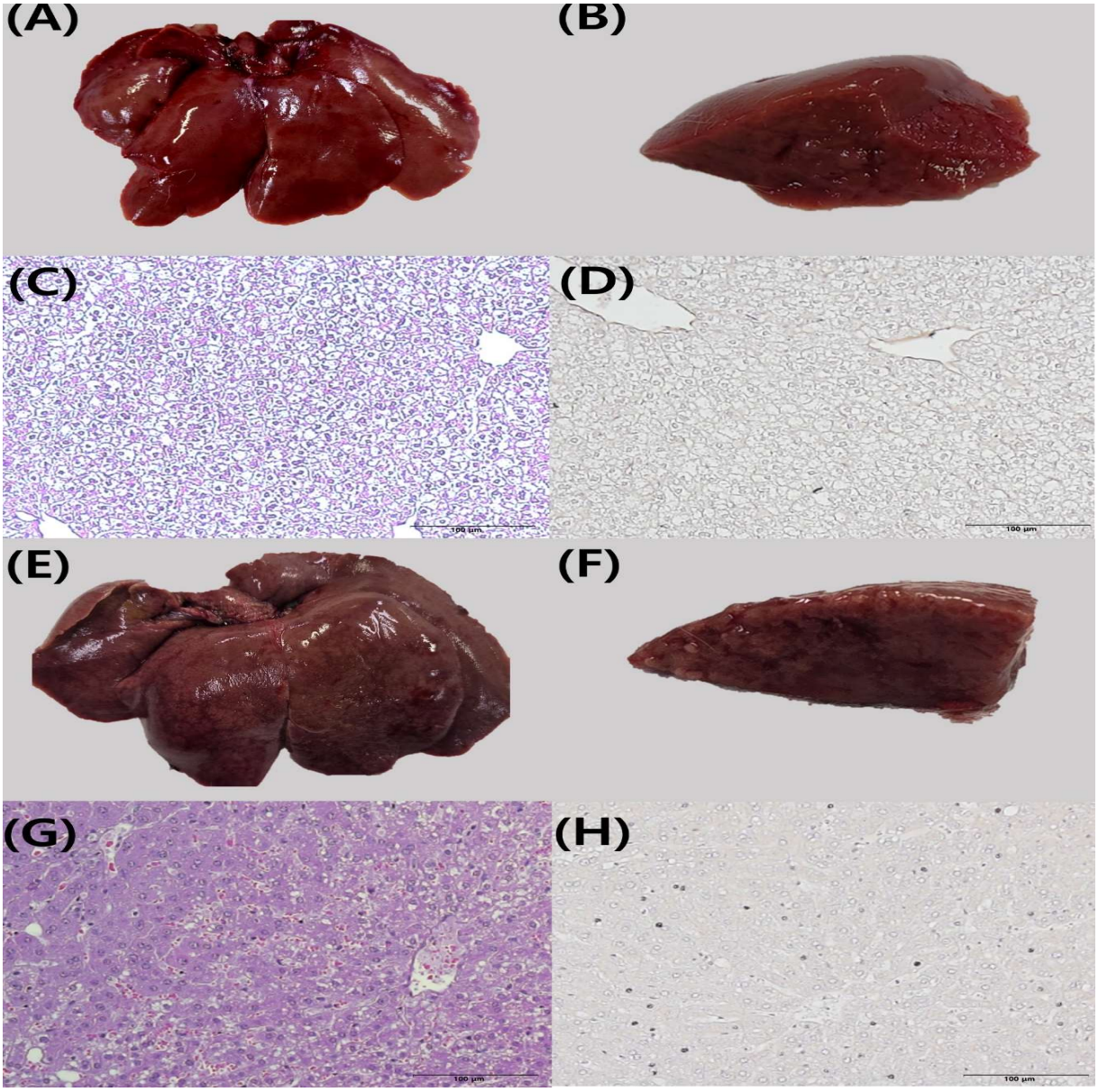

Fig. 7: Gross images, H&E staining, and Ki-67 immunostaining in the control and total lobar embolization groups**.** (A) and (B): Gross and cross-sectional liver images from the control group (N/S injection). (C) and (D): H&E and Ki-67 staining of liver tissue from the control group, respectively (×200); (E) and (F): Gross and cross-sectional images of the liver following total lobar embolization, showing multiple small white-grey nodules. (G): H&E staining of the embolized liver showing vacuolization, congestion, and partial necrosis (×200). (H): Ki-67 staining in the embolized liver, highlighting numerous brown-stained hepatocyte nuclei indicative of proliferation (×200).

Liver regeneration was evaluated via anti-Ki-67 immunostaining of control (Fig. 7D) and Group L (Fig. 7H) rabbits. The median Ki-67 proliferation index was 2.14 (range, 1.78–3.26) in the control group and 23.61 (range, 17.14–27.54) in Group L, with a significant difference between groups ($P<0.05$).

Table 5: Serial changes in liver enzymes and hematological parameters at pre-and 24-h post-embolization in the control group and Group L

		Control (n=3) Median (Min-Max)		Group L (n=10) Median (Q1-Q3)	
	Reference range	Pre	Post	Pre	Post
ALT (U/L)	32 - 129	30.00 (25.00-35.00)	57.00 (57.00-59.00)	53.00 (51.00-56.00)	139.00* (89.00-366.50)
AST (U/L)	16 - 100	17.00 (16.00-18.00)	27.00 (25.00-28.00)	28.00 (18.50-31.50)	159.00* (92.50-315.50)
ALP (U/L)	39 - 131	323.00 (296.00-350.00)	334.00 (330.00-378.00)	360.00 (315.00-369.50)	270.00 (244.50-301.50)
GGT (U/L)	12 - 22	8.00 (6.00-11.00)	14.00 (11.00-17.00)	10.00 (10.00-10.05)	11.00 (9.50-11.00)
RBC ($10^6/\mu L$)	4.45 - 6.71	5.78 (5.60-5.95)	5.65 (5.54-5.76)	6.04 (5.65-6.21)	6.28 (5.86-6.59)
HCT (%)	29.4 - 40.9	36.4 (35.20-37.5)	35.70 (34.78-36.62)	39.20 (36.35-40.35)	39.10 (37.20-42.85)
WBC ($10^3/\mu L$)	4.54 - 10.22	9.18 (6.39-11.96)	9.49 (7.15-12.25)	8.12 (7.56-9.15)	7.45 (7.17-9.32)

*P<0.05 (pre- vs. 24h post-embolization, Wilcoxon rank test). ALT, alanine aminotransferase; AST, aspartate aminotransferase; ALP, alkaline phosphatase; GGT, gamma-glutamyl transpeptidase; RBC, red blood cell count; HCT, hematocrit; WBC, white blood cell count.

DISCUSSION

In the pilot study, residual effects of gadoxetate disodium influenced semi-quantitative parameters (iAUC60, Max. slope, CER, and PEI), whereas quantitative parameters (K_{trans}, V_e) and time-based parameters (TTP and MTE) showed non-significant differences between sequential and gadolinium alone administration. This discrepancy could be attributed to the nature of each parameter. Quantitative parameters were derived from pharmacokinetic modeling, which estimates the transfer and distribution of contrast agents between the vascular compartment and extravascular extracellular space (EES) using the arterial input function (AIF). Considering that gadoxetate is largely cleared from the vascular compartment within 15 minutes (Choi *et al*, 2016), its effect on the arterial input function was likely minimal. Therefore, the observed differences between control group and Group L are likely attributable to the nature of intervention rather than variations in imaging conditions.

In the control group, mild elevation of liver enzymes was observed within the normal range, except for ALP. Preprocedural ALP levels were elevated across all groups, whereas other liver function tests remained within normal limits. This increase in ALP levels is likely age-related, as the rabbits were young (90–105 days) rather than indicative of hepatic dysfunction. Elevated ALP levels in young rabbits are commonly attributed to active bone growth, whereas ALT and AST remain within normal limits because they primarily reflect hepatocellular, not skeletal, activity (Melillo, 2007). In addition, non-significant imaging changes were detected on CT or MRI, suggesting minimal alterations from hepatic arterial access alone, such as hemorrhage or vascular injury. Nevertheless, CT immediately after embolization showed elevated baseline hepatic attenuation on pre-contrast scans due to residual angiography for hepatic arterial access, normalizing at 24h in controls, whereas changes persisted at 24h in group L due to embolic material.

On CT imaging immediately post-embolization, Group L showed significant differences from pre-embolization values in all phases except the arterial phase, likely due to the increased pre-contrast attenuation from hyper-attenuating lipiodol deposition and residual iodinated contrast, reducing HU ratio in the portal venous and delayed phases. At 24h post-embolization, the residual contrast had cleared, lowering pre-contrast HU compared to immediately post-embolization, but values remained elevated relative to pre-embolization levels owing to persistent lipiodol retention. Continued HU ratio reduction in the portal venous and delayed phases likely reflects secondary lipiodol effects or parenchymal injury induced by embolization. However, CT alone could not distinguish between these possibilities, requiring MRI. Minimal arterial phase change may reflect to the 20% of arterial blood supply of liver (Konstantinidis *et al.*, 2023).

On conventional MRI images, non-significant changes were observed in most cases. Hypointense areas on T1- and T2-W_fs in some cases resulted from lipiodol, which is composed of a mixture of ethyl esters, appears hyperintense on both T1- and T2-weighted images (Rauf *et al.,* 2023). However, the effect of lipiodol on MRI signals in clinical settings remains controversial. Some studies argue that its influence is negligible because of the low concentrations used in conventional TACE (Kubota *et al.,* 2001), whereas others have reported hypointensity on T1-W_fs and hyper-intensity on T2-W images in cases where lipiodol uptake covers 50–90% of the tumor volume (Lee *et al.*, 2016).

Lipiodol may also cause signal alterations in dual-phase imaging, including hyperintensity in in-phase and that in out-of-phase sequences (Lee *et al.*, 2016). In this study, normal liver tissue was used, and the lipiodol concentration was presumed to be lower than that typically observed in tumors, possibly resulting in less prominent effects. Visual changes on T1-W dual-phase images were not observed; however, a significant increase in PDFF (%) was observed both immediately and 24h post-embolization, suggesting that lipiodol may have contributed to some of the observed alterations (Yin *et al.*, 2012). Previous studies have shown that a PDFF value >6.4% may indicate hepatic steatosis (Luo *et al.*, 2018). However, in this study, a median PDFF value of 6.32% was observed in spite of the absence of hepatic steatosis after embolization. This suggests that caution is needed when interpreting PDFF values after embolization, as lipiodol may cause false positives for fatty liver disease. Additional large-scale studies are needed to clearly elucidate the effects of lipiodol on MRI signal characteristics across various sequences and tissue types.

Gadoxetate enhanced MRI revealed non-significant visual parenchymal changes in any phase except the hepatobiliary phase, which showed distinct hypointensity useful for assessing liver injury. Quantitative SI analysis showed significant changes in all phases. The decrease in SI

in the pre-contrast phase after embolization was attributed to lipiodol deposition, whereas in the postcontrast phase, SI decreased significantly immediately after embolization. As it was observed before the onset of hepatic injury, this change is thought to reflect decreased perfusion due to vascular occlusion by embolic agent (van Riel *et al.*, 2016). The decrease in signal intensity persisted across all phases at 24 hours after embolization, likely due to decreased perfusion caused by embolization and decreased contrast uptake due to functional hepatocyte loss (Lee *et al.*, 2022). Histopathological examination supported these findings, confirming liver damage in most cases.

In the present study, gadoxetate-enhanced MRI detected early hepatic damage, whereas conventional MRI showed non-significant changes immediately after or 24-h post-embolization. These findings are consistent with those of a previous study (Watanabe *et al.*, 2011). This is due to the use of a liver-specific contrast agent, which enables the assessment of liver function and quantitative comparison of SI across different phases. In this study, no bile leakage or common bile duct stricture was observed during the hepatobiliary phase, and the biliary tract was found to be intact.

In DCE-MRI, Quantitative parameters such as K_{trans}, K_{ep}, $V_{e,}$ and V_p are commonly used. However, in this study, only K_{trans} and V_e were included, while K_{ep} and V_p were considered unreliable. K_{trans} represents the rate at which the contrast agent moves from the blood vessels to the EES and serves as a measure of the wash-in process. It is less sensitive to noise and motion artifacts, which likely explains its high reproducibility in highly perfused tissues such as the liver, spleen, and pancreas (Holland *et al.,* 2022). In contrast, K_{ep} reflects the rate at which the contrast agent diffuses back from the EES into the blood vessels, making it more susceptible to noise and motion artifacts. In addition, rabbits have much higher heart and respiratory rates than humans, which likely exacerbated these effects. V_p , which represents the blood plasma volume fraction, exhibited low reproducibility owing to its low signal-to-noise ratio (SNR; Holland *et al.*, 2022).

The absolute values of quantitative DCE-MRI parameters are challenging to compare across studies unless the analysis methods are carefully standardized (Ng *et al.*, 2015). In fact, even in normal rabbit liver, reported K_{trans} values have shown considerable variability, ranging from $0.09\pm0.07 min^{-1}$ (Park *et al.*, 2015) to $0.184\pm0.086 min^{-1}$ (Chen *et al.*, 2016) and up to $0.45\pm0.07 min^{-1}$ (Liu *et al.,* 2020), depending on the study. Therefore, rather than relying on absolute values reported in previous studies, we evaluated intra-individual trends, and similarly observed significant decrease in K_{trans} immediately after embolization in group L, consistent with present study (Saito *et al*., 2018). This decrease can be attributed to the embolic agent blocking blood flow, reducing blood supply to the liver, which is turn reduces perfusion and slows down the delivery of contrast agent to the tissue. Regarding V_e, which represents the EES fraction, its relationship with embolization has not been well-established in the literature. In this study, non-significant changes in V_e were observed in the short term after embolization. This could be due to the fact that the cellular structure remains intact during coagulative necrosis of hepatocytes, making changes in V_e not immediately apparent. Moreover, the decreased SNR due to hypoperfusion after embolization may have contributed to the decreased analysis accuracy, obscuring the changes in V_e.

Also, semi-quantitative indices derived from the DCE-MRI SI curves showed significant changes after embolization. In group L, significant decrease in parameters such as iAUC60, CER, PEI, and Max. slope was observed immediately after embolization. This likely reflects decreased arterial perfusion due to a decrease in both the amount and rate of contrast agent delivery to the tissue (Park *et al.,* 2015). Furthermore, a significant increase in TTP was observed immediately after embolization, likely due to delayed contrast delivery due to impaired perfusion.

Unlike normal liver, most tumors rely primarily on arterial blood flow. Although this is a unique vascular physiology, intra-arterial embolization can cause severe liver injury through ischemia of the surrounding liver tissue, leading to hypoxia and free radical production, causing hepatocyte necrosis and liver dysfunction (Barros *et al.*, 2001). At 24h after embolization, a significant increase in ALT and AST levels was observed in Group L, likely due to hepatocyte damage. Cell edema, congestion, vacuolar degeneration and mild necrosis were observed upon histopathological (H&E) examination.

However, liver regeneration typically peaks approximately 24h after injury and is largely completed by 72h (Ishikawa *et al.,* 2021). The Ki-67, a nuclear protein expressed during active phases of the cell cycle but absent in quiescent cells, is a well-established marker of cellular proliferation. In our study, Ki-67 immunohistochemistry revealed a clearly increased number of positively stained nuclei in Group L compared to that in the controls, suggesting active liver regeneration, consistent with previous findings (Wang *et al*., 2011). The increase in perfusion observed on MRI at 24-h post-embolization was presumed to result from a combination of hepatic arterial redistribution and regenerative liver responses.

This study had some limitations. First, to minimize anesthesia time and ensure imaging at a consistent time point, MRI was performed immediately after CT. Although iodinated contrast agents have minimal or no interference with MRI signal characteristics (Morales *et al.*, 2016), minor effects cannot be entirely excluded. Second, the control group had a small sample size (n=3), which may have reduced validity of the statistical analysis. However, this minimized unnecessary animal use per ethical principles. Furthermore, previous studies showed intra-arterial normal saline infusion alone does not induce significant hepatic or systemic changes in rabbit, supporting the validity of using a minimal number in the control group (Zhang *et al.*, 2022). In spite of the small sample, the control group exhibited consistent results across time. Another limitation is the short observation period, limited to immediately after embolization and the subsequent 24h. The results of this study showed that hepatic perfusion returned to near baseline levels within 24 hours, suggesting minimal further changes after this time point. Long-term studies are needed to confirm whether the early recovery of hepatic perfusion and function is sustained and not followed by delayed hepatocellular injury and recurrent perfusion impairment.

Conclusions: In conclusion, this study demonstrated that lipiodol alone, even at clinically relevant doses, induces hepatic injury in normal liver tissue through hypoperfusion. However, compensatory perfusion redistribution and hepatic regeneration were observed within 24h. Furthermore, DCE-MRI is more sensitive and accurate in detecting these early perfusion alterations than CT, conventional MRI, and gadoxetate-enhanced MRI. Although such embolization may be tolerable by patients with sufficient healthy liver reserve, caution is warranted in those with limited remnant liver volume or impaired hepatic function, as lipiodol alone can cause ischemic damage. In such cases, DCE-MRI may serve as a valuable tool for monitoring post-embolization hepatic hemodynamics.

Acknowledgments: This research was supported by National University Development Project (Glocal University 30 project) at Jeonbuk National University in 2024.

Authors contribution: SP and HY conceived the idea, designed the study, conducted the experiments and analyzed the data. EN, BS and KL assisted in the experimental work by offering constructive advice and guidance. All authors interpreted results, reviewed the manuscript, and approved the final version.

REFERENCES

Baleato-González S, Vilanova JC, Luna A, *et al.,* 2023. Current and advanced applications of gadoxetic acid–enhanced MRI in hepatobiliary disorders. Radiographics 43(4):e220087. https://doi.org/10.1148/rg.220087

Barros LF, Stutzin A, Calixto A, *et al.,* 2001. Non-selective cation channels as effectors of free radical-induced rat liver cell necrosis. Hepatology 33(1):114-22. https://doi.org/10.1053/jhep.2001.20976

Breit HC, Vosshenrich J, Heye T, *et al.,* 2023. Assessment of hepatic function employing hepatocyte specific contrast agent concentrations to multifactorially evaluate fibrotic remodeling. Quantitative Imaging in Medicine and Surgery13(7): 4284-4294.

Chen J, Qian T, Zhang H, *et al.,* 2016. Combining dynamic contrast enhanced magnetic resonance imaging and microvessel density to assess the angiogenesis after PEI in a rabbit VX2 liver tumor model. Magnetic Resonance lamging 34(2):177-82. https://doi.org/10.1016/j.mri.2015.10.021

Chen YW, Tsai MY, Pan HB, *et al*., 2014. Gadoxetic acid-enhanced MRI and sonoelastography: Non-invasive assessments of chemoprevention of liver fibrosis in thioacetamide-induced rats with Sho-Saiko-To. Public Library of Science One 9(12):e114756. https://doi.org/10.1371/journal.pone.0114756

Choi Y, Huh J, Woo DC, *et al.,* 2016. Use of gadoxetate disodium for functional MRI based on its unique molecular mechanism. British Journal of Radiology 89(1058):20150666. https://doi.org/10.1259/bjr.20150666

de Graaf W, van den Esschert JW, van Lienden KP, *et al.*, 2011. A rabbit model for selective portal vein embolization. Journal of Surgical Research 171(2):486-94. https://doi.org/10.1016/j.jss.2011.05.015

Deschamps F, Farouil G, Gonzalez W, *et al.,* 2017. Stabilization improves theranostic properties of lipiodol®-based emulsion during liver trans-arterial chemo-embolization in a VX2 rabbit model. Cardiovascular and Interventional Radiology 40(6):907-13. https://doi.org/10.1007/s00270-017-1581-3

Holland MD, Morales A, Simmons S, *et al.,* 2022. Disposable point-of-care portable perfusion phantom for quantitative DCE-MRI. Medical Physics 49(1):271-81. https://doi.org/10.1002/mp.15341

Huang YS, Chiang JH, Wu JC, *et al.,* 2002. Risk of hepatic failure after transcatheter arterial chemoembolization for hepatocellular carcinoma: predictive value of the monoethylglycinexylidide test. American Journal of Gastroenterology 97(5):1223-7. https://doi.org/10.1111/j.1572-0241.2002.05709.x

Ishikawa J, Takeo M, Iwadate A, *et al.,* 2021. Mechanical homeostasis of liver sinusoid is involved in the initiation and termination of liver regeneration. Communications Biology 4(1):409. https://doi.org/10.1038/s42003-021-01964-w

Kacała A, Dorochowicz M, Patrzałek D, *et al.,* 2023. Safety and feasibility of transarterial bleomycin–lipiodol embolization in patients with giant hepatic hemangiomas. Medicina 59(8):1358.

Keller S, Chapiro J, Brangsch J, *et al.*, 2020. Quantitative MRI for assessment of treatment outcomes in a rabbit VX2 hepatic tumor model. Journal of Magnetic Resonance Imaging 52(3):668-85. https://doi.org/10.1002/jmri.27026

Konstantinidis AO, Patsikas MN, Papazoglou LG, *et al.,* 2023. Congenital portosystemic shunts in dogs and cats: Classification, pathophysiology, clinical presentation and diagnosis. Veterinary Sciences10(2):160. https://doi.org/10.3390/vetsci10020160.

Kubota K, Hisa N, Nishikawa T, *et al.,* 2001. Evaluation of hepatocellular carcinoma after treatment with transcatheter arterial chemoembolization: comparison of Lipiodol-CT, power Doppler sonography, and dynamic MRI. Abdominal Imaging 26(2):184-90. https://doi.org/10.1007/s002610000118

Lawson A, Kamarajah SK, Parente A, *et al.,* 2023. Outcomes of trans-arterial embolisation (TAE) vs transarterial chemoembolisation (TACE) for hepatocellular carcinoma: A systematic review and meta-analysis. Cancers (Basel) 15(12):3166. https://doi.org/10.3390/cancers15123166

Lee BC, Jeong YY, Heo SH, *et al.,* 2022. Gadoxetic acid-enhanced MRI features for predicting treatment outcomes of early hepatocellular carcinoma (<3cm) after trans-arterial chemoembolization. Academic Radiology 29(9):e178-e188. https://doi.org/10.1016/j.acra.2021.10.012.

Lee MJ, Kim MJ and Baek SY, 2016. MRI findings of Lipiodol uptake in hepatocellular carcinomas: a focus on signal intensity. Ewha Medical Journal 39(4):110-7.

Liang W, Greven J, Qin K, *et al.*, 2022. Sulforaphane exerts beneficial immunomodulatory effects on liver tissue via a Nrf2 pathway-related mechanism in a murine model of hemorrhagic shock and resuscitation. Frontiers in Immunology 13: 822895.

Liu HF, Wang Q, Du YN, *et al*., 2020. Dynamic contrast-enhanced MRI with Gd-EOB-DTPA for the quantitative assessment of early-stage liver fibrosis induced by carbon tetrachloride in rabbits. Magnetic Resonance Imaging 70:57-63. https://doi.org/10.1016/j.mri.2020.03.016

Luo RB, Suzuki T, Hooker JC, *et al.* 2018. How bariatric surgery affects liver volume and fat density in NAFLD patients. Surgical Endoscopy 32(4):1675-82. https://doi.org/10.1007/s00464-017-5846-9

Mahmoodiyan A and Mahboubizadeh S, 2025. Recent progress in biomaterial–enhanced transarterial embolization for primary liver cancer therapy: A short review. Progress in Chemical and Biochemical Research 8:191-207.

Melillo A, 2007. Rabbit clinical pathology. Journal of Exotic Pet Medicine16(3):135-45. https://doi.org/10.1053/j.jepm.2007.04.006

Miyayama S, Mitsui T, Zen Y, *et al.,* 2009. Histopathological findings after ultraselective transcatheter arterial chemoembolization for hepatocellular carcinoma. Hepatology Research39(4):374-81. https://doi.org/10.1111/j.1872-034X.2008.00464.x

Morales H, Lemen L, Samaratunga R, *et al.,* 2016. Effects of iodinated contrast on various magnetic resonance imaging sequences and field strength: implications for characterization of hemorrhagic transformation in acute stroke therapy. World Journal of Radiology8(6):588. https://doi.org/10.4329/wjr.v8.i6.588

Nagayama Y, Inoue T, Kato Y, *et al*., 2021. Relative enhancement ratio of portal venous phase to unenhanced CT in the diagnosis of lipid-poor adrenal adenomas. Radiology 301(2):360-8. https://doi.org/10.1148/radiol.2021210231

Nakao N, Uchida H, Kamino K, *et al.,* 1994. Determination of the optimum dose level of lipiodol in transcatheter arterial embolization of primary hepatocellular carcinoma based on retrospective multivariate analysis. Cardiovascular and Interventional Radiology 17:76-80. https://doi.org/10.1007/BF00193921

Ning E and Wang Z, 2020. Effect of intrahepatic arterial delivery of Sorafenib on normal liver tissue of rabbit: An experimental study. Journal of Advanced Medical Sciences 3(1):1-10. https://doi.org/10.30564/jams.v3i1.1468

Ng CS, Wei W, Bankson JA, *et al.,* 2015. Dependence of DCE-MRI biomarker values on analysis algorithm. Public Library of Science One 10(7):e0130168. https://doi.org/10.1371/journal.pone.0130168

Ozaki K, Tanahashi Y and Goshima S, 2026. Gadoxetic acid-enhanced MRI in hepatocellular carcinoma: a comprehensive review of diagnostic, surveillance, and treatment response prediction and assessment. Japanese Journal of Radiology 44(1):2-23. https://doi.org/10.1007/s11604-025-01870-x

Park HS, Han JK, Lee JM, *et al.,* 2015. Dynamic contrast-enhanced MRI using a macromolecular MR contrast agent (P792): Evaluation of antivascular drug effect in a rabbit VX2 liver tumor model. Korean Journal of Radiology 16(5):1029-37. https://doi.org/10.3348/kjr.2015.16.5.1029

Rata M, Khan K, Collins DJ, *et al.,* 2021. DCE-MRI is more sensitive than IVIM-DWI for assessing anti-angiogenic treatment-induced changes in colorectal liver metastases. Cancer Imaging 21(1):67. https://doi.org/10.1186/s40644-021-00436-0

Rauf M, Rana AI, Anwar J, *et al.,* 2023. A review of MRI appearances of lipiodol in conventional TACE (cTACE) treated hepatocellular carcinomas. Journal of Ayub Medical College Abbottabad 35(4 (Suppl 1):740-45.

Reeder SB, Cruite I, Hanuktib G, *et al.*, 2011. Quantitative assessment of liver fat with magnetic resonance imaging and spectroscopy. Journal of Magnetic Resonance Imaging 34(4):729-49. https://doi.org/10.1002/jmri.22775.

Reynolds HM, Tadimalla S, Wang YF, *et al*., 2022. Semi-quantitative and quantitative dynamic contrast-enhanced (DCE) MRI parameters as prostate cancer imaging biomarkers for biologically targeted radiation therapy. Cancer Imaging 22(1):71. https://doi.org/10.1186/s40644-022-00508-9

Saito K, Ledsam J, Sugimoto K, *et al.,* 2018. DCE-MRI for early prediction of response in hepatocellular carcinoma after TACE and sorafenib therapy: a pilot study. Journal of the Belgian Society of Radiology 102(1):40. https://doi.org/10.5334/jbsr.1635

Sharma R, Inglese M, Dubash S, *et al.,* 2020. Monitoring response to transarterial chemoembolization in hepatocellular carcinoma using 18F-fluorothymidine PET. Journal of Nuclear Medicine 61(12):1743-8. https://doi.org/10.2967/jnumed.119.240598

van Riel WG, van Golen RF, Reiniers MJ, *et al.,* 2016. How much ischemia can the liver tolerate during resection? Hepatobiliary Surgery and Nutrition 5(1):58-71. https://doi.org/10.21037/hbsn.2016.02.04

Wang Y, Zheng C, Liang B, *et al.,* 2011. Hepatocellular necrosis, apoptosis, and proliferation 554 after transcatheter arterial embolization or chemoembolization in a standardized rabbit 555 model. Journal of Vascular and Interventional Radiology 22(11):1606-12. https://doi.org/556 10.1016/j.jvir.2011.07.030

Watanabe H, Kanematsu M, Goshima S, *et al.,* 2011. Staging hepatic fibrosis: Comparison of gadoxetate disodium–enhanced and diffusion-weighted MR imaging—preliminary observations. Radiology 259(1):142-50. https://doi.org/10.1148/radiol.11101862

Yin X, Guo Y, Li W, *et al.,* 2012. Chemical shift MR imaging methods for the quantification of transcatheter lipiodol delivery to the liver: Preclinical feasibility studies in a rodent model. Radiology 263(3):714-22. https://doi.org/10.1148/radiol.12111916.

Zaarour Y, Derbel H, Tran C, *et al*., 2024. Evaluation of a new beads reflux control microcatheter in drug-eluting bead trans-arterial chemoembolization. Research in Diagnostic and Interventional Imaging 10: 100048

Zhang H, Ren Y, Li H, *et al*., 2022. Renal and hepatic artery embolization with pickering gel emulsion of lipiodol in rabbit. BioMed Central Cancer 22:1300. https://doi.org/10.1186/s12885-022-10337-5